PHYSICAL REVIEW B VOLUME 47, NUMBER 15 15 APRIL 1993-I

Effect of substrate-imposed strain on the growth of metallic overlayers calculated for fcc and hcp iron

T. Kraft, M. Methfessel, M. van Schilfgaarde,* and M. Scheffler
Fritz-Haber-Institut der Max-Planck-Gesellschaft, Faradayweg 4-6, D-14195 Berlin, Germany
(Received 5 August 1992; revised manuscript received 23 October 1992)

By means of electronic-structure calculations with use of the full-potential linear-muffin-tin-orbital method and the local spin-density approximation (LSDA), the influence of the substrate-imposed strain on a fcc (111) or hcp (0001) iron layer is determined. A careful treatment of the elastic effects predicts that the nonmagnetic hcp structure is more stable than the nonmagnetic fcc structure for a wide range of lattice constants but becomes less favorable for a large positive or negative strain on the overlayers. The stabilization of the fcc structure at large mismatches is traced to the stiffer hcp interplanar bonds, a consequence of the decreased axial c/a ratio. It is argued that similar behavior should be found for the other transition metals. The results are prototypical for the substrate-overlayer elastic interaction but cannot be compared directly to experiment because of systematic LSDA errors in the magnetic-ferromagnetic energy difference for iron.

I. INTRODUCTION

The properties of transition-metal overlayers on substrates consisting of other metals are of large interest both experimentally and theoretically. An especially fascinating point is that the overlayers can sometimes be forced into a structure which is distinct from that of the equilibrium bulk by a suitable choice of the metal substrate. To a large extent, this is a consequence of the condition that the in-plane lattice constants of the two materials must be commensurate if growth is to be epitaxial. One obtains, in this way, materials such as bcc Pd (Ref. 1) and bcc Ag (see, for example, Ref. 2 and references therein). Additional interest results from the fact that the magnetic state of the overlayer metal is often influenced by the structure. A system which has been studied experimentally in the past is iron grown on the transition metals Ru (Refs. 3 and 4), Cu (Ref. 5), and Ag.[6] Despite intense experimental effort the structure and the magnetic ordering of the Fe overlayers are not yet clear in some cases and theoretical studies are warranted.

The quantity of interest is the energy of the Fe overlayers as a function of the substrate interatomic spacing. Of the different effects which are relevant hereby, of primary importance is the elastic energy which is needed to distort the Fe layers to match them to the substrate. We focus on this aspect in this paper. To obtain a realistic picture, other energy contributions must also be considered. First, there is the interface energy, which depends on the type of bonding which Fe can undergo with the substrate atoms. Second, there will be some influence due to the surface energy. For very thin overlayers, these two terms can become as important as the elastic energy. For thick layers, on the other hand, the elastic energy will dominate. In addition to these energy contributions, the picture can again change if the dynamics of the growth process is included. For instance, the first phase of the overlayer growth involves separated Fe atoms adsorbed on the substrate, followed by an Fe monolayer. The geometry adopted in this step can influence the positions of the atoms in the subsequently deposited layers. Nevertheless, despite these complications we feel that it is important to first understand the basic elastic contribution to the total energy before an investigation of the more complicated phenomena is undertaken. For the case of Fe considered in this paper, an additional complication arises because the local spin-density approximation (LSDA) does not predict the ground state of the bulk material correctly; the energy of the magnetic phases comes out systematically too high by at least 15 mRy (see Sec. III A). As a consequence, our calculations do not obtain magnetic structures as favorable even when the mismatch to the substrate is large. This is in disagreement with recent experimental results.[7,5] We reconsider the consequences of the inherent LSDA error at the end of Sec. III A.

In an attempt to clarify the question of the elastic properties of the competitive strained iron phases, we have calculated total energies for bulk hcp and fcc iron for various cases of tetragonal elastic distortions by means of the spin-polarized full-potential linear-muffin-tin-orbital method using the LSDA (Refs. 8 and 9) within density-functional theory. This approach permits an accurate description of energy changes due to lattice distortions. Of the different possible quasihexagonal alignments on a hcp (0001) substrate, we focus here on the competition between the hcp (0001) and fcc (111) stacking sequence of the close-packed hexagonal planes. By using a spin-polarized code we permit a magnetic moment to appear if this should be energetically favorable; however, one result of the calculations is that both the fcc and hcp phases are nonmagnetic for all reasonable interatomic distances around the equilibrium geometry.

The organization of the paper is as follows. In Sec. II we give a brief description of the FP-LMTO method.

In Sec. III we show some results concerning the ground state of iron, a question which has been frequently discussed over the last years.[10–13] The question of the LSDA ground state was resolved by a recent full-potential linear augmented plane-wave (FLAPW) calculation.[10] We use this as a test case of our method (without, however, considering gradient corrections[14–16]) to determine the intrinsic LSDA error when comparing magnetic with nonmagnetic ground states (Sec. III A). This error is the origin of the favor of nonmagnetic phases in our calculations. By relaxing the interlayer spacing, we calculate in Sec. III B the total energies for the fcc and hcp structure as a function of the prescribed in-plane interatomic distance and draw conclusions concerning the adopted stacking sequence. To explain our results in simple terms, we reproduce them using a bond-strength model in Sec. III C. Conclusions can be found in Sec. IV.

II. DESCRIPTION OF THE METHOD

The calculations described in this work were performed using the full-potential linear-muffin-tin-orbital method. As in the atomic-sphere approximation (ASA), the basis set consists of atom-centered Hankel functions augmented by means of numerical solutions of the Schrödinger equation inside the atom-centered "atomic spheres." However, in distinction to the ASA method the atomic spheres are not taken as overlapping and the charge density and potential can have a completely general shape in the interstitial region as well as inside the atomic spheres. An accurate treatment in the interstitial region is achieved by an interpolation technique which matches a linear combination of Hankel functions to the values and slopes on the spheres. This procedure is applied to the interstitial charge density, the partial densities which are products of two basis functions, and the exchange-correlation potential and energy density. The accuracy of the approach is comparable to that of the FLAPW method for reasonably close-packed systems. For details, we refer to previous publications.[17–19] In the present case, LMTO's with three different localizations (given by the Hankel envelope-function kinetic energies -2.3, -1.0, -0.7 Ry) of s, p, and d character were used leading to a basis of 27 functions per atom. A scalar-relativistic formulation is used. For the spin-dependent local-density approximation to the exchange-correlation functional we used the Ceperley-Alder form[20] in the Vosko-Wilk-Nusair parametrization.[21] The $\mathbf{k}$-space sampling was done on an uniform mesh of 145 irreducible $\mathbf{k}$ points for bcc and fcc iron and 135 for hcp iron, respectively. The energy eigenvalues were broadened by 20 mRy using Gaussian smearing. Sphere radii were chosen to be 3% smaller than touching in the unrelaxed structure to allow lattice distortions.

III. RESULTS

A. The ground state of iron

To comment on previous predictions of the ground state of bulk iron and as a test for our method, we have calculated total energies for nonmagnetic fcc and bcc and for ferromagnetic bcc iron as a function of the atomic volume. The results are shown in Fig. 1.

The minimum of the ferromagnetic bcc curve is the reference energy for the others. From our data, we obtain the equilibrium Wigner-Seitz radii and lattice constants, bulk moduli, cohesive energies, and magnetic moments which are compared to other calculated values and to experiment in Table I. We find the ferromagnetic bcc phase energetically favored by $\Delta E = 19.5\,\mathrm{mRy/atom}$ compared to the paramagnetic bcc phase, but the paramagnetic fcc phase again $\Delta E' = 5.9\,\mathrm{mRy/atom}$ lower than the ferromagnetic bcc phase. The FLAPW results for these energy differences are 17.6 and 7.9 mRy/atom,[10] in good agreement with our results. A local-density-approximation (LDA) calculation using the LMTO-ASA method gave the corresponding values of 16.5 and 6.5 mRy/atom.[11] A calculation using the augmented-spherical-wave (ASW) method[22] determined the nonmagnetic (NM) fcc phase to be marginally higher in energy than the ferromagnetic (FM) bcc phase, whereas the NM hcp structure was lowest in energy by 3.6 mRy/atom compared to the FM bcc. The fact that the FM bcc phase becomes favored compared to other studies mentioned above could be found in the spherical averaging used in the ASW method; however, this should also hold for the above-cited LMTO-ASA study. The question of the energy difference of fcc and hcp iron in our present work is carefully addressed in Sec. III B. So far, our calculations reproduce the previously found result, namely that the LSDA predicts the ground state of iron incorrectly. This is a consequence of the fact that the exchange-correlation functional is taken from the homogeneous electron gas.[13] For the case of iron, it has been demonstrated that nonlocal contributions to the exchange-correlation potential in the form of gradient corrections are able to predict the correct ground state.[10–12,23] Because our calculations do not apply any further noticeable numerical or technical approximations, we conclude the LDA-LSDA error in

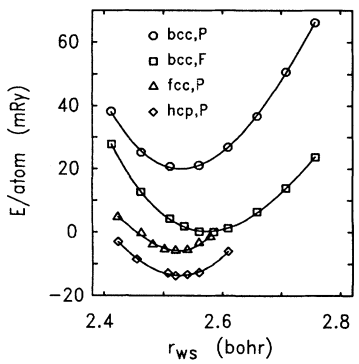

FIG. 1. Calculated total energies of iron as a function of the Wigner-Seitz radius r_{WS} for the paramagnetic (P) bcc, fcc, and hcp structure as well as for the ferromagnetic (F) bcc phase. Energies are relative to the minimum of the ferromagnetic bcc curve. Symbols indicate the calculated energies. The curves are fits with fifth-order polynomials.

TABLE I. Comparison of various calculated ground-state properties of bcc Fe with experimental values and with previous calculations obtained using the LMTO-ASA method, the augmented-spherical-wave (ASW) method and the (full-potential) linear augmented-plane-wave method. Listed are the equilibrium lattice constant a, the magnetic moment m at equilibrium, the cohesive energy E_c, and the bulk modulus B for the paramagnetic and ferromagnetic phase. All tabulated results are in the LSDA without gradient corrections. Zero point vibrations are not included.

Case	a (Å)	m (μ_B)	E_c (eV)	B (Mbar)	Method
para	2.71		8.50	3.20	FP-LMTO
ferro	2.77	2.02	7.73	2.52	(this work)
para	2.73		5.79	3.06	LAPW[a]
ferro	2.82	2.15		2.14	ASW[b]
para	2.72				FLAPW[c]
ferro	2.78	2.08	7.32	1.74	
para	2.70				LMTO-
ferro	2.75	2.23	6.96	1.53	ASA[d]
ferro	2.86	2.21	4.31	1.68	Expt.

[a]Reference 28.
[b]Reference 29.
[c]Reference 10.
[d]Reference 11.

describing ferromagnetic states of iron to be at least 15 mRy/atom. The phases considered in Sec. III B turn out to be nonmagnetic, so that the failure of the LSDA when comparing energies for magnetic and nonmagnetic structures is not expected to affect our conclusions concerning the effect of strain. However, the error must be taken into account when transferring our results to a realistic experimental situation of iron grown on a surface.[7,5]

B. The influence of the in-plane lattice constant on the structure of relaxed Fe phases

The question to be addressed here is to what extent the structure of close-packed metallic phases can be influenced by the lattice constant which is imposed by the substrate. As a simple example, materials which normally crystallize in the bcc structure can be forced into a fcc structure and vice versa by a suitable choice of the substrate lattice constant. A more subtle question arises when the imposed lattice constant is compatible with the interatomic distance in the close-packed hexagonal planes which constitute both the hcp and the fcc structure. In that case, the formation as either a fcc (111) or hcp (0001) crystal is conceivable, depending on the stacking sequence adopted by successive planes. For thick layers where surface and interface effects become negligible, the choice between these competitive structures is influenced by three factors. As a first approximation, the energy difference should be that between the hcp and fcc structures when both are at their respective equilibrium lattice constants. This matter has been thoroughly investigated in the past and it is now known that for transition metals, it is essentially the d-band filling which determines the hcp-fcc energy difference.[24] Secondly, the elastic properties of the hcp and fcc materials determine the energy cost when the overlayers deform to match the substrate interatomic spacing, where this is not equal to the ideal value. The sum of both energy contributions determines the overlayer structure, which could thus depend on the imposed lattice constant via the strain energy. Finally, energy contributions due to magnetic ordering could change this picture in a fundamental way. In the following, we investigate this question for the case of Fe using accurate spin-polarized total-energy calculations. It turns out that for all overlayer geometries considered here, the magnetic phase lies higher in energy so that an unrestricted LSDA calculation moves into the nonmagnetic state. By experience, the LDA is known to predict reliable elastic properties for non-magnetic systems. Since we are comparing structures which are more similar in terms of the nearest-neighbor coordination than in the fcc-bcc ground-state discussion and, more importantly, magnetic effects do not play a role in this context, we are assuming that the local-density approximation is appropriate to the hcp-fcc energy difference despite the failure of the LSDA for the iron ground state (see Sec. III A). Our results concerning the elastic effects are the first step in a detailed description of the overlayer growth process, which should ultimately include growth dynamics as well as interface and surface effects.

First, we discuss the hcp-fcc energy difference of Fe when each structure is at its respective equilibrium lattice spacing. In both structures, Fe becomes nonmagnetic in the LSDA. For transition metals, previous theoretical considerations[24] have shown the connection between the power moments

$$\mu_r = \int_{-\infty}^{\infty} (E - \varepsilon_d)^r n_d(E)\, dE \tag{1}$$

and the structural energy difference. Here, $n_d(E)$ denotes the density of states for the d electrons and ε_d the on-site d orbital energy. It was shown quite generally that the hcp-fcc energy difference must go through zero

at least twice as a function of the d-band filling. From the fact that the first nonidentical moment is μ_4, a general shape of the hcp-fcc energy difference was deduced as shown in Fig. 2. For the d-band filling of iron of 6 d electrons, the hcp structure is predicted lower in energy. Ducastelle and Cyrot-Lackmann[24] not only derived the overall behavior of the hcp-fcc energy difference but also the general property that transition metals with a negative hcp-fcc energy difference will further lower their energy by a reduction of the axial ratio c/a from the ideal value of $\sqrt{8/3} = 1.63$. Conversely, metals with the fcc structure lower in energy would want to have c/a larger than ideal when forced into a hcp structure. This will be relevant for the discussion at the end of Sec. III.

Self-consistent LDA calculations concerning this point were presented in Ref. 25 which confirmed the results of the moment theory, as well as of a work based on a force theorem in the LMTO-ASA method.[26] These *ab initio* calculations showed that for Fe the hcp-fcc difference is largest compared to other $3d$ metals and hcp is most stable. For hcp Fe, we have minimized the energy as a function of both the lattice constant and the c/a ratio. The nearest-neighbor distance for fcc and hcp comes out almost the same, namely 4.54 and 4.53 a.u. for hcp and fcc, respectively. The axial ratio in the hcp structure is found to be $c/a = 1.58$ which equals the value calculated in Ref. 25. Our calculations again confirm the moment theory and the previous LDA results. For an isotropic change in volume and a fixed axial ratio of $c/a = 1.58$ for the hcp structure, we find the hcp phase energetically favored by $\Delta E = 7.9\,\mathrm{mRy/atom}$ (Fig. 3). In conclusion, if only isotropic distortions are taken into account, the hcp stacking sequence is clearly favored. This picture could well change when more general distortions are permitted.

To this aim we present the results of a more thorough investigation. For an accurate description, a full-potential method is essential to obtain reliable results. We proceed in a way analogous to that which would be used by an experimentalist; that is, we simulate the experimental growth of Fe on a close-packed substrate with a prescribed lattice constant. We choose an in-plane nearest-neighbor distance d_{nn}. Keeping this value fixed, we vary the axial ratio c/a to map out the total energy as a function of the distance d_z between adjacent lattice planes. From the minimum of the total energy we obtain, for this value of d_{nn}, the relaxed interplanar spacing and the total energy at the minimum. This procedure is then repeated for several values of d_{nn} for both structures. Considering both hcp and fcc structures as hexagonal but with different stacking sequences, we are varying the in-plane atomic distance as a parameter and determining the c/a ratio from the minimum of the total energy. The range of c/a and d_{nn} is limited by the requirement that the atomic spheres may not overlap when the lattice deformation is applied. Figure 4 shows the "raw data" obtained in this way for hcp Fe. Each curve displays the total energy as a function of c/a for one fixed value of d_{nn}. In agreement with the discussion of the axial ratio

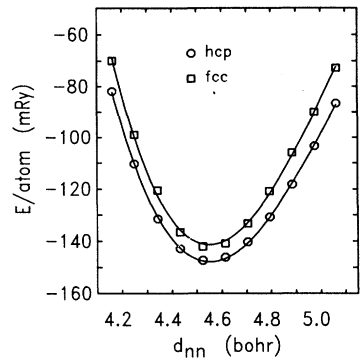

FIG. 3. Total energy per atom for hcp and fcc Fe as a function of the interatomic distance d_{nn} in the fcc(111) and hcp(0001) plane for isotropic volume change. The c/a ratio was fixed at 1.58 for hcp and at the ideal value of 1.633 for fcc. Only the mRy part is shown; for hcp, the total energy is -2451.148 Ry. The hcp structure is lower in energy by $\Delta E = 7.9\mathrm{mRy/atom}$ at equilibrium.

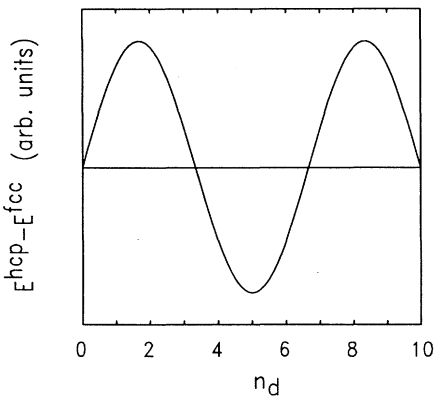

FIG. 2. Qualitative behavior of the hcp-fcc energy difference as a function of the d-band occupation as deduced from the moment theory (Ref. 24). Assigning a d charge of 6 to Fe, the hcp structure is predicted to be more stable.

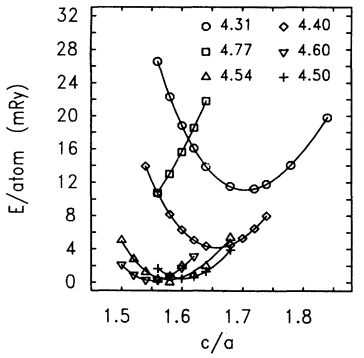

FIG. 4. Total energy per atom for hcp Fe as a function of the axial c/a ratio for various values of the in-plane lattice constant d_{nn}. Energies are relative to the relaxed hcp structure at $d_{\mathrm{nn}} = 4.538$ bohr and $c/a = 1.58$.

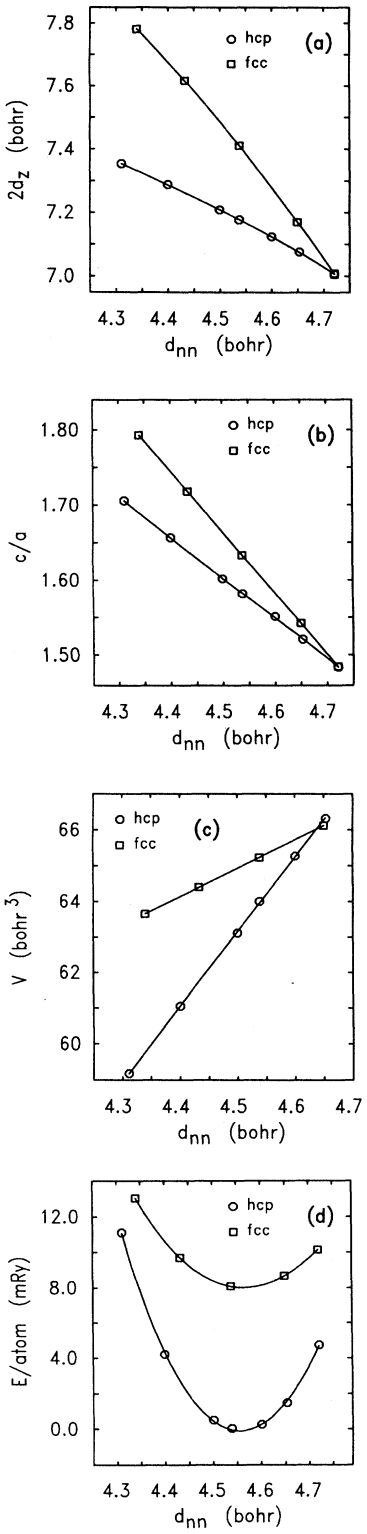

FIG. 5. Calculated values for (a) twice the interplanar spacing, (b) the c/a ratio, (c) the atomic volume, and (d) the total energy per atom for the relaxed hcp and fcc structures as a function of the in-plane nearest-neighbor distance d_{nn}. At equilibrium, the hcp phase is found to be energetically favored, whereas the fcc phase would be lower in energy when d_{nn} is larger or smaller by roughly $\pm 10\%$ or more.

of hcp Fe above, the absolute minimum of the energy is attained for a lattice constant $d_{nn} = 4.538$ bohr and a c/a ratio of 1.58. The corresponding fcc curves are very similar except that, because of the cubic symmetry, the absolute energy minimum lies at the ideal c/a ratio of 1.633 with $d_{nn} = 4.510$ bohr.

To obtain a clearer picture we plot a number of quantities extracted from Fig. 4 as a function of d_{nn} in Figs. 5(a)–5(d): the interplanar spacing d_z, the c/a ratio $2\,d_z/d_{nn}$, the atomic volume V, and the total energy per atom E of the relaxed structure. For both structures, d_z and c/a decrease approximately linearly as d_{nn} increases. This shows that the crystal tries to maintain the atomic volume close to the equilibrium value by compensating the in-plane expansion with a compression in z direction. Here, one observes a relevant difference between the two structures, which is also evident from the behavior of the atomic volume shown in Fig. 5(c). For the fcc structure, the volume increases only slightly with the in-plane lattice constant, while the increase for hcp is twice as large. This shows that the hcp structure is "stiffer" than fcc respective to a tetragonal c/a distortion. The effect on the total energy can be seen in Fig. 5(d) which can be considered as the main result of these calculations. For d_{nn} close to the equilibrium interatomic distances in hcp and fcc Fe (about 4.54 bohr), the hcp structure is lower in energy by the previously discussed value of 7.9 mRy/atom. When d_{nn} is varied to smaller or larger values, the increase of energy in the hcp case is larger than in fcc as a consequence of the higher stiffness of the hcp lattice. Thus, for extreme values of d_{nn} the fcc structure becomes more favorable and fcc growth should be observed. However, Fig. 5(d) shows that the mismatch to the equilibrium lattice constant must be approximately $\pm 10\%$ before this happens. However, growth at the mismatches for which we find the hcp-fcc crossover is hardly possible without introducing defects such as dislocations, steps, kinks, and islands. Therefore, the result of our calculation is that the hcp phase is clearly favored over fcc for all feasible lattice constants, but we also find the theoretically interesting result that a transition to fcc is in principle possible. Also, similar behavior is plausible for other materials for which the hcp-fcc energy difference could be smaller, thus making a transition between structures possible at more reasonable mismatches. We return to this question at the end of Sec. III C.

To compare our results to an experimental situation,

TABLE II. Calculated values for the lattice stiffness $\partial^2 E/\partial \varepsilon^2$ for hcp and fcc Fe in mRy. The third column shows the results from LDA calculations, the fourth the results using the bond-strength model with the bond stiffness taken from the isotropic volume change of fcc Fe. For both strain modes, the hcp structure is stiffer than the fcc structure.

Strain mode	Structure	FP-LMTO	Model
(a) $\delta l_1 = 0$	hcp	6499	6167
	fcc	2710	3256
(b) $\delta V = 0$	hcp	6040	5518
	fcc	3308	3583

we recall again that the LSDA obtains nonmagnetic phases too low by at least $\sim 15\,\mathrm{mRy/atom}$. It is reasonable to assume that a ferromagnetic structure should in fact be favored when the substrate interatomic spacing is large since this phase has a larger equilibrium lattice constant than the NM phase. The elastic energy penalty to match to the substrate lattice would therefore be less. This is compatible with experimental indications of magnetic Fe overlayer phases.[7,4]

C. Origin of the enhanced stiffness in the hcp structure

In the previous section we found the Fe hcp and fcc structures to exhibit different behavior with respect to a tetragonal c/a distortion, with the result that the transition from hcp to fcc is in principle possible for extreme cases of the lattice constant mismatch. In the following we trace the origin of the different elastic behavior to the reduced c/a ratio in the hcp structure. To gain more insight, we consider two distinct distortions. First, as case (a), strain is applied in the direction orthogonal to the close-packed plane without changing the in-plane interatomic distance. This distortion changes the unit-cell volume and is the one which was investigated in Sec. III B. Second, we also examine the related volume-conserving shear as case (b), in which the expansion of the interplanar spacing is accompanied by a contraction of the in-plane interatomic distance. In both cases, we parametrize the distortion in such a way that the c axis is multiplied by $(1+\varepsilon)$. The in-plane atomic distance remains unchanged in case (a) and scales with $1/\sqrt{1+\varepsilon}$ in case (b). In the following we will also abbreviate these distortions by "$\delta l_1 = 0$" and "$\delta V = 0$," respectively, where l_1 denotes the in-plane bond length.

To leading order, the crystal energy is a quadratic function of the strain parameter ε. Of interest is the lattice stiffness, which is the second derivative $\partial^2 E/\partial\varepsilon^2$ at $\varepsilon = 0$. This quantity is proportional to a certain combination of the second-order elastic constants.[27] Our calculated values for the second derivative are shown in the second-to-last column of Table II. For case (a), hcp is found stiffer by a factor of more than 2. This quantifies the behavior already discussed in connection with Fig. 5(d). Distortion (a) changes the lengths of only the out-of-plane bonds (which are tilted by 35.3° to the c axis). These are shorter in the hcp structure due to the nonideal c/a ratio. Therefore, a possible explanation for the increased hcp stiffness is that the shortened bonds have become harder. For the volume-conserving case (b), the situation is more complicated because the distortion changes the length of the in-plane as well as of the out-of-plane bonds. For hcp compared to fcc, the former are longer and therefore could be expected to be softer. It is not clear *a priori* whether the bond hardening overcomes the bond softening. Our calculations obtain hcp harder for this distortion too, but by a smaller amount than in case (a).

In such a model, the relevant ingredient is the dependence of the bond stiffness (that is, $\partial^2 B/\partial l^2$ where B is the bond strength) on the bond length l. Assuming that this is a well-defined and transferable property for a given material, we can obtain $\partial^2 B/\partial l^2$ as $\frac{1}{12}\partial^2 E/\partial l^2$ at any desired bond length l from the calculated isotropic energy-volume curve for bulk fcc Fe. The bond strength and stiffness which were obtained in this way are shown in Figs. 6(a) and 6(b). Note that the $B(l)$ curve is asymmetric around its minimum. For lengths larger than the equilibrium distance, the increase of the energy is smaller than in the case when l is shortened by the same amount; that is, it costs more energy to compress a bond than to expand it.

If we now shear the fcc or the hcp lattice, we have to take two different lengths into account. These are the in-plane length l_1 and the out-of-plane length l_2. The overall stiffness of the lattice is given by

$$\frac{\partial^2 E}{\partial\varepsilon^2} = N_1\frac{\partial^2 B(l_1)}{\partial\varepsilon^2} + N_2\frac{\partial^2 B(l_2)}{\partial\varepsilon^2} \quad , \tag{2}$$

where N_1 and N_2 denote the number of in-plane and out-of-plane bonds, respectively. Note that in these cases, l_1 is identical to the nearest-neighbor distance in the close-packed hexagonal plane, d_{nn}.

The fcc and hcp structures have $N_1 = N_2 = 6$. Because we consider strains around the equilibrium geometry, the first derivative $\partial B/\partial l_i$ is zero, and by chain differentiation we obtain

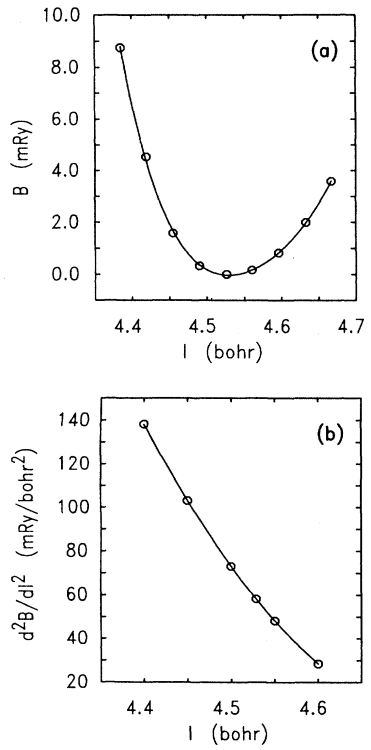

FIG. 6. (a) Bond strength $B(l)$ and (b) stiffness $\partial^2 B/\partial l^2$ as deduced from an isotropic volume change of the fcc structure. Note that the bond stiffness increases strongly as the bond length l is decreased.

$$\frac{\partial^2 E}{\partial \varepsilon^2} = N_1 \left(\frac{\partial l_1}{\partial \varepsilon}\right)^2 \frac{\partial^2 B}{\partial l^2}\bigg|_{l=l_1} + N_2 \left(\frac{\partial l_2}{\partial \varepsilon}\right)^2 \frac{\partial^2 B}{\partial l^2}\bigg|_{l=l_2} . \tag{3}$$

This expression is built up out of purely geometric factors [the quadratic terms $(\partial l_i/\partial \varepsilon)^2$] and the bond stiffnesses $\partial^2 B/\partial l^2$ at the lengths l_1 and l_2.

The out-of-plane and in-plane lengths involved in the two distortion cases are

$$l_1 = \begin{cases} a_0 , & \delta l_1 = 0 \\ a_0/\sqrt{1+\varepsilon} , & \delta V = 0 , \end{cases} \tag{4}$$

$$l_2 = \begin{cases} a_0 \sqrt{\frac{1}{3} + \left(\frac{c_0}{a_0}\right)^2 \frac{(1+\varepsilon)^2}{4}} , & \delta l_1 = 0 \\ a_0 \sqrt{\frac{1}{3(1+\varepsilon)} + \left(\frac{c_0}{a_0}\right)^2 \frac{(1+\varepsilon)^2}{4}} , & \delta V = 0 , \end{cases} \tag{5}$$

where a_0 denotes the in-plane interatomic distance at $\varepsilon = 0$ and c_0/a_0 the corresponding axial ratio. In the fcc case or for hcp at the ideal axial ratio, the geometric factors are given for the distortion with $\delta l_1 = 0$ by

$$\frac{\partial l_1}{\partial \varepsilon}\bigg|_{\varepsilon=0} = 0 , \tag{6}$$

$$\frac{\partial l_2}{\partial \varepsilon}\bigg|_{\varepsilon=0} = \frac{a_0}{2} , \tag{7}$$

and for the distortion with $\delta V = 0$ by

$$\frac{\partial l_1}{\partial \varepsilon}\bigg|_{\varepsilon=0} = -\frac{a_0}{2} , \tag{8}$$

$$\frac{\partial l_2}{\partial \varepsilon}\bigg|_{\varepsilon=0} = \frac{a_0}{2} .$$

For hcp at the calculated equilibrium axial ratio of 1.58, $\partial l_i/\partial \varepsilon$ shows only slight and irrelevant deviations from these values. The important ingredient is that the *bond stiffnesses* are substantially different for the various bond lengths, namely

$$l_1(\text{fcc}) = l_2(\text{fcc}) = 4.510\,\text{bohr} : \quad \frac{\partial^2 B}{\partial l^2} = 68.0\,\text{mRy} , \tag{9}$$

$$l_1(\text{hcp}) = 4.538\,\text{bohr} : \quad \frac{\partial^2 B}{\partial l^2} = 61.2\,\text{mRy} , \tag{10}$$

$$l_2(\text{hcp}) = 4.439\,\text{bohr} : \quad \frac{\partial^2 B}{\partial l^2} = 116.8\,\text{mRy} . \tag{11}$$

Inserting the values from Eqs. (6)–(10) in Eq. (3), we are now able to compare these results from the model with those of the accurate LDA calculation. For the lattice stiffnesses in the hcp and fcc structures, we obtain the values in the last column of Table II. For the distortion with $\delta l_1 = 0$, the model correctly exhibits the much larger stiffness of the hcp structure. From Eq. (4) and the fact that $\partial l_1/\partial \varepsilon$ is zero for this distortion, it is clear that the origin of the effect is that $\partial^2 B/\partial l^2$ for the out-of-plane bonds is twice as large for the shorter bonds in the hcp structure. Thus, as suggested above, the reduced hcp c/a ratio is the underlying reason for the increased hcp stiffness in this distortion. Moreover, it is interesting that not only the trend but also the absolute values of $\partial^2 E/\partial \varepsilon^2$ are rather well reproduced. Having thus gained confidence, one can inspect the more complicated case of the volume-conserving distortion. From Eqs. (6) and (7) it follows that the softening of the in-plane bonds and the hardening of the out-of-plane bonds when the nonideal hcp c/a ratio is adopted cancel to a large extent, since the changes of the in-plane and out-of-plane bond lengths have opposite signs. It is less obvious that the cancellation would be complete if the relation between bond length and stiffness were to be a linear function. This follows from Eq. (7) which shows that the bond length changes are exactly equal but opposite for the volume-conserving shear. Consequently, the *overall* bond stiffness for the hcp lattice would be equal to that of fcc if the relation were linear. The increase in stiffness in our calculations for hcp is therefore a consequence of the rapidly increasing stiffening of the bond as its length is reduced. In terms of the fcc-energy volume curve, it is the third-order term in the expansion of the bulk energy around the equilibrium lattice constant which is finally responsible for the effect.

Can these conclusions be transferred to other materials, or are they only valid for the special case of iron? In fact, it is easy to see that the basic pattern of Fig. 5(d) should be the same for the other transition metals. That is, whichever phase (fcc or hcp) has the lower energy at equilibrium not only has a c/a ratio lower than the ideal value but is also the one which is stiffer relative to the c/a distortion. This follows from the general behavior of the axial ratios, as deduced from the moment description. For those metals which have hcp as the most favorable phase, the c/a ratio is smaller than ideal and the whole argument holds as above. Conversely, in those cases for which fcc is the more stable phase at equilibrium, the hcp c/a ratio is larger than the ideal value[25] and hcp will then be softer with respect to the c/a shear. In either case, the fcc and hcp energies must cross when the distortion becomes large enough. Thus, the transition between the two structures is in principle always possible by varying the substrate lattice constant. However, whether this is possible for a distortion which can be actually realized without inducing defects can only be answered by a more detailed investigation in each case.

IV. CONCLUSIONS

In this paper we have used accurate local-density calculations to analyze the effects of overlayer strain on the stacking sequence when iron can grow in either the fcc (111) or the hcp (0001) structure. The two relevant ingredients are the hcp-to-fcc energy difference at equilibrium and the elastic shear energy which is required to match the crystal to a nonideal lattice constant. For iron, the energetically more favorable structure at the equilibrium

lattice constant was calculated to be nonmagnetic hcp. This is in agreement with earlier theories, based on the moments of the d-band density of states, which trace the hcp stability to the number of d electrons. With respect to the tetragonal c/a distortion which would be needed to match the iron overlayers to a nonideal substrate lattice constant, we find nonmagnetic hcp Fe approximately twice as stiff as nonmagnetic fcc Fe. This implies a crossing of the hcp and fcc total energies at large lattice mismatches. The larger stiffness of the hcp structure was explained in a simple model which obtains the stiffness of the nearest-neighbor Fe–Fe bond as a function of the bond length from the fcc energy-volume curve. The central effect was identified as to be the hardening of the hcp out-of-plane bonds due to the bond shortening by the decreased axial c/a ratio. From general considerations, it follows that all transition metals should exhibit a similar transition between the hcp and fcc structures at some substrate lattice constant. However, whether the transition is feasible for realistic strains will depend on the material in question. Unfortunately, the transfer of our results to the real experimental situation is restricted by the fact that surface and interface effects were not considered and also by the LSDA error when comparing magnetic and nonmagnetic phases. Nevertheless, our careful analysis of the strain effects is a necessary first step for an accurate description of the overlayer growth process.

ACKNOWLEDGMENTS

We thank P. M. Marcus for discussion about the growth problem of iron on Ru(0001) and A. T. Paxton for helpful hints about the axial ratio of hcp transition metals.

*Permanent Address: SRI International, 333 Ravenswood Ave., Menlo Park, CA 94025.

[1]B. C. Bolding and E. A. Carter, Phys. Rev. B **44**, 3251 (1991).
[2]M. Said, F. Máca, K. Kambe, M. Scheffler, and N. E. Christensen, Phys. Rev. B **38**, 8505 (1988).
[3]M. Maurer, J. C. Ousset, M. F. Ravet, and M. Piecuch, Europhys. Lett. **9**, 883 (1989).
[4]D. Tian, H. Li, F. Jona, and P. M. Marcus, Solid State Commun. **80**, 783 (1991).
[5]P. Xhonneux and E. Courtens, Phys. Rev. B **46**, 556 (1992).
[6]Z. Q. Qiu, J. Pearson, and S. D. Bader, Phys. Rev. Lett. **67**, 1646 (1991).
[7]F. J. Himpsel, Phys. Rev. Lett. **67**, 2363 (1991).
[8]W. Kohn and L. J. Sham, Phys. Rev. **140**, A1133 (1965).
[9]L. Hedin and B. J. Lundquist, J. Phys. **C 4**, 2064 (1971).
[10]T. C. Leung, C. T. Chan, and B. N. Harmon, Phys. Rev. B **44**, 2923 (1991).
[11]P. Bagno, O. Jepsen, and O. Gunnarsson, Phys. Rev. B **40**, 1997 (1989).
[12]J. M. MacLaren, D. P. Clougherty, and R. C. Albers, Phys. Rev. B **42**, 3205 (1990).
[13]C. S. Wang, B. M. Klein, and H. Krakauer, Phys. Rev. Lett. **54**, 1852 (1988).
[14]J. P. Perdew, Phys. Rev. Lett. **55**, 1665 (1985).
[15]D. C. Langreth and M. J. Mehl, Phys. Rev. Lett. **47**, 446 (1981).
[16]J. P. Perdew and Y. Wang, Phys. Rev. B **30**, 4734 (1984).
[17]M. Methfessel, Phys. Rev. B **38**, 1537 (1988).
[18]M. Methfessel, C.O. Rodriguez, and O.K. Andersen, Phys. Rev. B **40**, 2009 (1989).
[19]M. Methfessel and M. Scheffler, Physica B **172**, 175 (1991).
[20]D. M. Ceperley and B. J. Alder, Phys. Rev. Lett. **45**, 566 (1980).
[21]S. H. Vosko, L. Wilk, and M. Nusair, Can. J. Phys. **58**, 1200 (1980).
[22]J. Kübler, Solid State Commun. **72**, 631 (1989).
[23]D. J. Singh, W. E. Pickett, and H. Krakauer, Phys. Rev. B **43**, 11 628 (1991).
[24]F. Ducastelle and F. Cyrot-Lackmann, J. Phys. Chem. Solids **32**, 285 (1971).
[25]A. T. Paxton, M. Methfessel, and H. M. Polatoglou, Phys. Rev. B **41**, 8127 (1990).
[26]H. Skriver, Phys. Rev. B **31**, 1909 (1985).
[27]M. Alouani, R. C. Albers, and M. Methfessel, Phys. Rev. B **43**, 6500 (1991).
[28]V. L. Moruzzi, J. F. Janak, and A. R. Williams, *Calculated Electronic Properties Of Metals* (Pergamon, New York, 1978).
[29]V. L. Moruzzi and P. M. Marcus, in *Handbook Of Ferromagnetic Materials*, edited by K. Buschow (Elsevier, Amsterdam, 1993), Vol. 7.